Correlation between time and angular alignment in molecular dynamics simulations of heavy ion collisions

B. Harvey,[1,2,3,*] M. Youngs,[1] A. B. McIntosh,[1] A. Jedele,[1,4] A. Abbott,[1,4] J. Gauthier,[1] K. Hagel,[1] A. Hannaman,[1,4] A. Hood,[1] K. Krieble,[3] Y.-W. Lui,[1] L. A. McIntosh,[1] A. Rodriguez Manso,[1] M. Sorensen,[1,4] Z. Tobin,[1,4] R. Wada,[1] A. Zarrella,[1,4] and S. J. Yennello[1,4]

[1]*Cyclotron Institute, Texas A&M University, College Station, Texas 77843, USA*
[2]*Physics Department, Texas A&M University, College Station, Texas 77843, USA*
[3]*Physics and Earth Science Department, Moravian College, Bethlehem, Pennsylvania 18018, USA*
[4]*Chemistry Department, Texas A&M University, College Station, Texas 77843, USA*

(Received 9 October 2020; accepted 11 December 2020; published 28 December 2020)

Neutron-proton equilibration is a process which has been used to study the density dependence of the symmetry energy term in the nuclear equation-of-state. This study utilizes constrained molecular dynamics (CoMD) simulations of ^{70}Zn + ^{70}Zn with collision energies of 35 and 45 MeV/nucleon. An algorithm is used which searches through CoMD events and identifies the PLF* after it separates from the target and determines its lifetime, Δt. It also determines the fragments that the PLF* breaks apart into and determines their angular alignment. This technique gives an opportunity to explore how the average alignment of dynamically produced fragments, $\langle\alpha\rangle_{\rm dyn}$, evolves with PLF* lifetime. An approximately linear relationship was determined with $d\langle\alpha\rangle_{\rm dyn}/d\Delta t = 0.98 \pm 0.08$ rad/zs and 1.06 ± 0.09 rad/zs for the 35 and 45 MeV/nucleon, respectively, indicating a correlation with magnitude consistent with classically determined values which were used for prior experimental studies.

DOI: 10.1103/PhysRevC.102.064625

I. INTRODUCTION

In intermediate energy heavy-ion collisions, nuclear matter far from equilibrium can be produced. This can result in shape deformations, density gradients, neutron-proton asymmetries, and nonuniformly excited nuclear matter. The properties of these exotic nuclear systems both affect and can be studied through the collision dynamics. Collision dynamics are guided by the nuclear equation-of-state (nEOS) which relates the thermodynamic properties of pressure, temperature, density, chemical potential, and internal energy [1,2]. The symmetry energy in the nEOS is the energy penalty associated with having excess nucleons of one type [3,4]. In particular, for nuclear systems with excess neutrons and extreme density gradients, the nuclear asymmetry energy influences neutron-proton equilibration, which in turn influences the collision dynamics [5].

This analysis investigates a dynamical breakup process known to occur in noncentral heavy ion collisions at intermediate energy using a theoretical model. This mechanism is illustrated in Fig. 1. If a collision is central, then multifragmentation is likely to occur, and if the collision is peripheral, then there is only modest perturbation of the projectile and target nuclei [6,7]. However, for midperipheral collisions, with impact parameter $b \approx 6$ fm, there is enough overlap between the projectile and target material to strongly deform them both without necessarily totally fragmenting the system [8,9]. For such collisions, a low density neck can form between the primary excited projectilelike fragment (PLF*) and the primary excited targetlike fragment (TLF*) as these two bodies begin to separate from each other [10,11]. The symmetry energy is density dependent and drives excess neutrons to this low-density region [12].

Figure 1 illustrates the low-density, relatively neutron-rich region (blue) and the near saturation density, less neutron-rich regions of the PLF* and TLF* (red). Eventually, the PLF* breaks from the TLF*, carrying some portion of the neutron-rich neck with it. At this point the PLF* is a strongly deformed excited large nuclear fragment with regions of varying neutron excess; it also can contain some significant amount of angular momentum. This may be true of the TLF* as well, but since the daughters of the PLF* are easier to observe experimentally we focus on the PLF*. Within the PLF*, the nucleons may rearrange to allow equilibration of the chemical potential (as well as shape, excitation, density, etc.); thus, the different regions of the PLF* may approach a more similar chemical potential as time progresses [13,14].

Due to the extreme deformation and velocity gradients, the PLF* can break apart dynamically into two sizable fragments [10,15–17] (also illustrated in Fig. 1) which we refer to as the heavy fragment (HF) and the lighter fragment (LF). Once these fragments are separated, chemical equilibration is halted between the HF and LF, as nucleons can no longer transfer between them. The longer the PLF* takes to break apart, the more time there is for nucleons to redistribute themselves

*bmharvey@tamu.edu

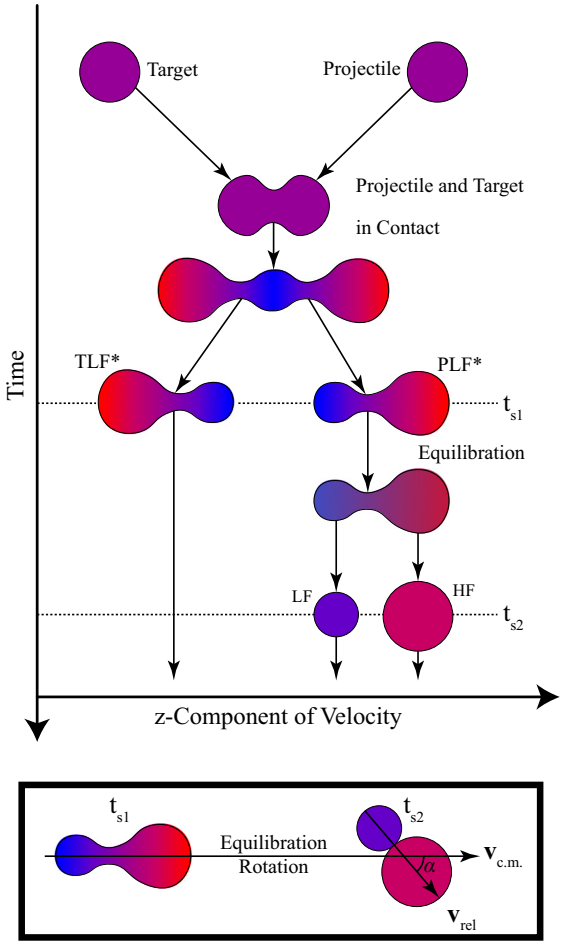

FIG. 1. Depiction of the breakup mechanism of interest in this work. Blue regions indicate regions of higher neutron density, and red regions indicate lower neutron density. PLF* rotation and neutron-proton equilibration take place between t_{s1} and t_{s2}. The alignment angle, α, is defined as the angle between the relative and center-of-mass velocity vectors.

within the PLF* toward chemical equilibrium. The LF in dynamically induced breakups most often originates from the neck region of the PLF* [10,14,18–21].

The LF is thus generally more neutron rich than the HF, but the longer it equilibrates with the HF the less neutron rich it becomes. Conversely, the HF is expected to become more neutron-rich. This implies that relative neutron-richness and the time between PLF* formation and breakup are correlated. Since angular alignment and the extent of equilibration are both dependent on the time of equilibration, the angular alignment is sensitive to the relative compositions of the LF and HF. Experimentally this timescale is infeasible to measure directly, but the angular alignment is thought to be a valid surrogate for time [13–15,18,22–27].

If the PLF* has angular momentum from its off-center collision with the target, then when it separates from the TLF*, it will rotate until it breaks apart again. Define t_{s1} to be the time when the PLF* separates from the TLF*, and let t_{s2} be the time when the PLF* breaks apart into the HF and LF. The amount of rotation of the PLF* during the time between t_{s1} and t_{s2}, Δt, can be assessed by the angle between the HF-LF relative velocity vector and the HF-LF center-of-mass velocity vector. This is defined to be the alignment angle, α, as shown in the lower portion of Fig. 1.

In recent experimental efforts, a general timescale of about 1–4 zs was established for neutron-proton equilibration using the velocities of the LF and HF [13,15,22,23,28]. Further support for the connection between α and the equilibration process of the PLF* was investigated via isoscaling parameters in Refs. [4,27,29,30]. These determinations of timescale are consistent with much earlier and recent assessments of nuclear breakup times [2,28,31–38]. Later experimental analysis in Refs. [14,25] used classical dynamics to approximate the angular velocity of the PLF* to link the alignment to the rate of neutron-proton equilibration. Work done with constrained molecular dynamics (CoMD) [39,40] in Ref. [23] has continued to reaffirm the direct relationship between Δt and α. The present work expands on using CoMD simulations to understand this correlation, and its dynamic origins.

II. EVENT TREE ANALYSIS

The angular alignment of the PLF* breakup can be determined experimentally by assuming that the two heaviest fragments detected forward of mid-velocity are the HF and LF, given they are each sufficiently heavy. This experimental assumption (E.A.) cannot be used to make any direct measurement of the total lifetime of the PLF*, during which equilibration can take place. Rather the timescale is extracted via other observables in the event based on the assumption that the HF and LF are properly identified. For this reason, a new method of identifying the PLF*, HF, and LF within CoMD simulations of heavy-ion collisions is used in this study. The following sections outline this analysis technique, and compares it to the technique which replicates the experimental assumptions.

This work uses two sets of 400 000 CoMD simulations each of ^{70}Zn + ^{70}Zn nuclear collisions over a triangular distribution of impact parameters ranging from 0 fm to the maximum impact parameter ∼10 fm. Both datasets used the medium stiffness parameter CoMD offers. The collision energies are the only differentiating feature of the two data sets and are 35 and 45 MeV/nucleon. The data collected from the CoMD simulations included the position, momentum, charge, and a unique identifier of each nucleon. For the purposes of this paper, time step refers to one of these output times. A clusterization routine was used which is based entirely on the nucleons' relative positions, considering nucleons with center-of-mass positions within 2.76 fm of each other to be part of the same fragment. This process also stores a unique identifier of each nucleon for the purposes of tracking the fragments through the simulation. The mass, proton number, center-of-mass position, and center-of-mass velocity of each cluster were then computed based on the properties of its constituent nucleons.

The composition of the fragments in one time step was used to determine its daughters in the next time step. Every fragment then has a lineage, a chain of fragments, in later time steps which contain its nucleons, which are its descendants.

It also has a lineage of nucleons in earlier time steps which contain its nucleons, defining its ancestors. These lineages are called the heaviest-daughter and heaviest-parent chains (HDCs and HPCs), respectively. This parent/daughter hierarchy of all of the fragments in an event is called the event tree and is the primary tool used to identify the PLF* and its decay. It allows for tracking every fragment precisely through the event and identifying which (if any) fragments at the end of the simulated event are correlated to PLF* breakup.

The event tree analysis begins by identifying the initial fragment which eventually breaks apart into the PLF* and TLF*. It is found by looking for a common descendant of the projectile and target. An algorithm is imposed to follow the heaviest-daughter chains of the projectile and target fragments until they merge and form a $Z \geqslant 50$ nucleus, as determined from the clustering routine. Here, two fragment chains merging is defined by the chains sharing a common fragment at any later time.

The HDC of the newly identified compound nucleus is tracked until a PLF*/TLF* separation is found. To find this separation, at each time step, the heaviest daughter is compared to the second heaviest daughter. If these fragments are found to satisfy the following conditions, then they are considered the PLF* and TLF*. It is required that the PLF* and TLF* are sufficiently large to break apart into smaller fragments later in the simulation [these fragments will be the HF and LF with Z requirements given in Eqs. (3) and (4)]. Thus, it is required that

$$Z_{\mathrm{PLF}^*}, Z_{\mathrm{TLF}^*} \geqslant 15. \tag{1}$$

In the center-of-mass frame, it is also required that the projections of the momenta of the PLF* and the TLF* onto the beam-line axis have opposing direction, or equivalently,

$$(p_{\mathrm{z,PLF}^*})(p_{\mathrm{z,TLF}^*}) < 0. \tag{2}$$

The fragment with the positive beam-line momentum is taken as the PLF*. Because the target and projectile have the same number of protons and neutrons, the event is later inverted and is registered as a new, statistically independent event with the PLF* identified as the fragment with opposing beam-line momentum. This technique effectively doubles the number of collisions in the data set, giving a total of 800 000 events for each collision energy. The event tree structure is utilized to add additional requirements to ensure that a complete TLF*/PLF* separation has occurred. The PLF* and the TLF* must have nonmerging heaviest-daughter chains (out to 1000 fm/c), and further must have nonmerging heaviest-parent-chains when starting at the last fragment in each of their HDCs. The first time step with a PLF* and TLF*, meeting the above requirements is considered t_{s1}. If the two fragments do not satisfy these conditions, then the heaviest daughter is compared to the third heaviest daughter and so on, until either a PLF*/TLF* pair is found or there are no more daughters in the current time step. In this latter case, the heaviest daughter is taken as the new compound fragment, and its daughters are searched for the PLF*/TLF* pair in a recursive manner.

If a PLF* is successfully identified in an event, then its HDC is then tracked in the same way as before to find fragments that qualify as the HF and LF. The only differences are the specific requirements used to accept or reject the PLF* breakup based on two of its daughters. It is now required that

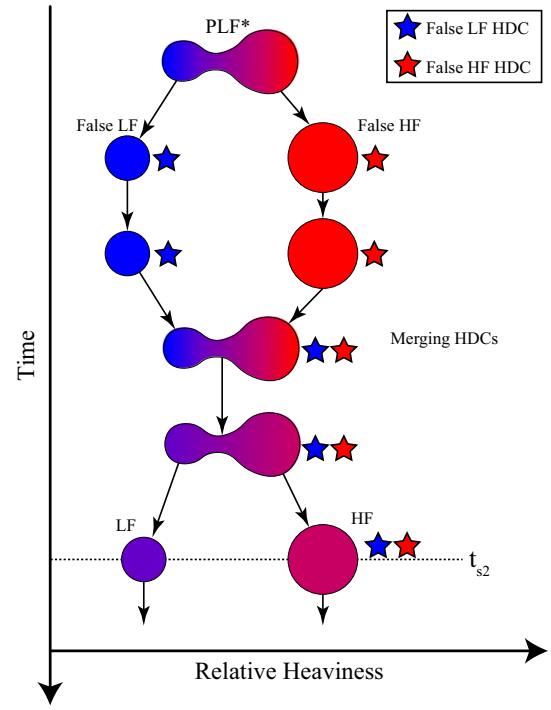

FIG. 2. Cartoon depicting merging heaviest-daughter chains. Equilibration and rotation persist until the HF and LF's last breakup. Here, blue and red coloring indicate relative neutron and proton richness, respectively.

$$Z_{\mathrm{HF}} \geqslant 11 \tag{3}$$

and

$$Z_{\mathrm{LF}} \geqslant 4. \tag{4}$$

The heavier fragment is determined primarily by Z. In the case two fragments have the same Z, ties are broken comparing first by total mass, and second by momentum in the beam-line direction p_z; larger values are attributed to heavier fragments in all cases. The nonmerging conditions of the PLF*/TLF* separation based on the event tree are similarly enforced for the HF/LF breakup. A depiction of merging HDCs is shown in Fig. 2. This cartoon shows first a PLF* recently separated from the target, highly deformed and with a relatively neutron-rich component, indicated by blue shading. The PLF* is then shown breaking apart into two fragments, one associated with the smaller, neutron-rich component, one associated with the heavier, less neutron-rich component. The fragments do not stay separated in this example, but rather merge again. The two components are still interacting, both in their combined motion and in their exchange of nucleons. At some time later this fragment may break apart again but with a new alignment and preferentially more equilibrated HF and LF. The proper identification of t_{s2} is necessary to ensure PLF* collective rotation and equilibration have both been effectively halted by complete breakup. This is why the

requirements against remerging are enforced in searching for PLF* breakup. If no PLF* breakup is found by 350 fm/c, then the event is dismissed in this analysis, as it is believed that the effects of dynamic decay are predominantly observed in CoMD by this point in the simulation [23]. After the HF and LF are identified as the daughters of the PLF*, they are tracked via their HDCs to $t = 350$ fm/c. At this point in the simulation there is barely a contribution to the overall yield from the dynamically decaying events (as will be verified later in Fig. 8). This is the time-step used to calculate α to make direct comparisons to the next method. Note that if the requirement against remerging HDCs is not imposed, it is possible that the HF and the LF could be falsely interpreted as the same fragment (see Fig. 2).

III. COMPARISON OF EXPERIMENTAL ASSUMPTIONS AND EVENT TREE ANALYSIS

It is impossible to collect the data used to construct the event trees analyzed by the previous method experimentally. Instead, an assumption is made that the heaviest two fragments forward of midvelocity are the HF and LF. To replicate those experimental assumptions with CoMD data, the fragments found at 350 fm/c are analyzed. If the heaviest two fragments forward of midvelocity at that time in the simulation satisfy $Z_{\mathrm{LF}} \geqslant 4$ and $Z_{\mathrm{HF}} \geqslant 11$, then their momenta and mass number are used to calculate α, as has been done in prior experimental work [14,25].

Figure 3(a) shows distributions of accepted events as a function of impact parameter using either one of the two analysis methods; data is shown for beam energies of 35 and 45 MeV/nucleon. Accepted events are those for which the analysis method identifies an HF and LF. Figure 3 shows raw yield of these events. The accepted events are dominated by midperipheral events, with maximum probability of acceptance at approximately 6 fm. The experimental assumptions are tolerant of more events, particularly at more central, violent collisions.

Figure 3(b) demonstrates this by normalizing for the effect of the triangular impact parameter distribution at each impact parameter. For both energies and methods, a peak is still observed around 6 fm, indicating that the cuts imposed are selective to not only midperipheral collisions, but to midperipheral events. This is consistent with the expectation that the breakup mechanism of interest primarily occurs for midperipheral collisions. At larger impact parameters, the accepted fraction drops to zero for both methods and energies since the perturbations are minor, and dynamically deformed PLF*s are not unlikely to be formed. For small impact parameters, the accepted fraction plateaus below 5% when the tree method is employed. The experimental assumptions lead to a much higher acceptance of events than the tree method for all impact parameters, but particularly at low impact parameters. In the most central, violent collisions, about 12% of the 35 MeV/nucleon collisions and 30% of the 45 MeV/nucleon collisions are accepted. If the central events typically have a different reaction mechanism than midperipheral events (as would be expected), then this implies that the experimental

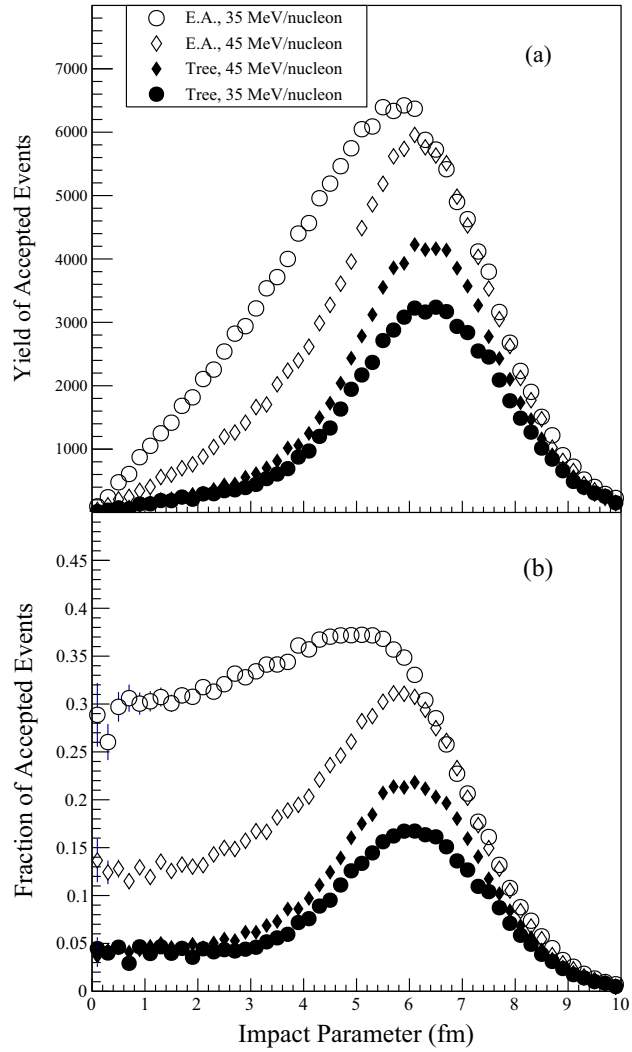

FIG. 3. (a) Yield of events accepted by the event tree analysis and the experimental assumptions (E.A.) and each energy as a function of impact parameter (out of 800 000 total events). (b) Same as panel (a), but normalized by the yield of total events for each impact parameter (following a triangular distribution).

analysis is not as selective to the reaction mechanism as the event-tree method is.

We can also compare the results of the angular alignment distributions, again separated by collision energy and analysis method. Formally, the angular alignment of the HF and LF fragments, α, is defined as

$$\alpha \equiv \arccos\left(\frac{\vec{v}_{\mathrm{c.m.}} \cdot \vec{v}_{\mathrm{rel}}}{|\vec{v}_{\mathrm{c.m.}}||\vec{v}_{\mathrm{rel}}|}\right), \tag{5}$$

where $\vec{v}_{\mathrm{c.m.}}$ is the center-of-mass velocity of the HF and LF given by

$$\vec{v}_{\mathrm{c.m.}} = \frac{(m_{\mathrm{HF}}\vec{v}_{\mathrm{HF}} + m_{\mathrm{LF}}\vec{v}_{\mathrm{LF}})}{m_{\mathrm{HF}} + m_{\mathrm{LF}}} \tag{6}$$

and the relative velocity is defined as

$$\vec{v}_{\mathrm{rel}} = \vec{v}_{\mathrm{HF}} - \vec{v}_{\mathrm{LF}}. \tag{7}$$

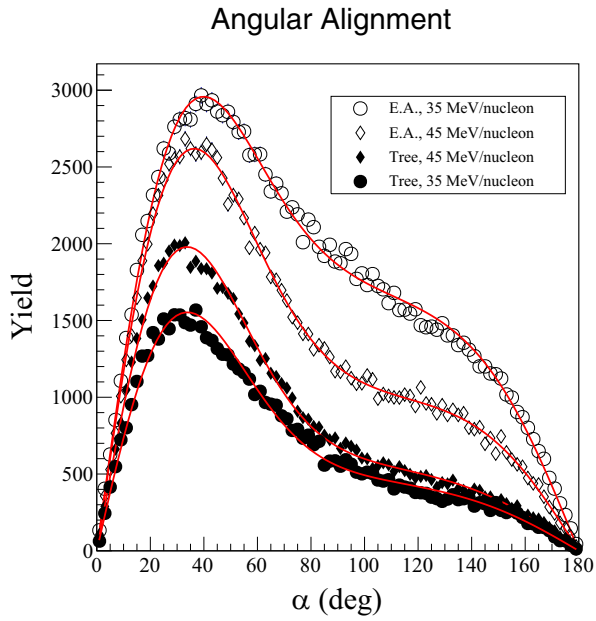

FIG. 4. Angular alignment distributions found by the event tree analysis and experimental assumptions for 35 and 45 MeV/nucleon collisions. Each distribution is fit to a model accounting for isotropic decay, dynamic breakup, and flipped dynamic events.

The distributions of angular alignments for each energy and method are shown in Fig. 4. This figure shows each data set fit with a function, which will be discussed later, in the formulation of Eq. (9). A definite peak associated with dynamic breakup processes is present at approximately 35 to 40° for each distribution which rises above a symmetric statistical distribution of alignments. We see that the contribution to this dynamic peak is higher relative to the statistical yield, which must be symmetric about 90°, with the event-tree method, while the overall yield is higher under the experimental analysis method. This suggests that the event tree method is more selective than the experimental assumption in discriminating the dynamical reaction mechanism, consistent with the conclusions drawn from Fig. 3. The qualitative shape of all of these distributions is in agreement with prior experimental work, which describes a dynamic peak rising above an approximately sinusoidal statistical background [14,25]. We expand on the models used in these prior works to try to characterize these distributions in more detail.

To further understand how the experimental assumptions may differ from the event-tree method, one can also compare events where a PLF* breakup was identified by both methods. In these cases, a direct comparison of the calculated angular alignments are plotted in Fig. 5. This will provide further insight into the structure of the one-dimensional distributions in Fig. 4. Since there are two methods used to find α, we refer to the angular alignment calculated with the tree method as α_{tree}, and with the experimental assumptions as $\alpha_{\text{E.A.}}$. As expected, there is general agreement between each method with a primary peak filled along the $\alpha_{\text{tree}} = \alpha_{\text{E.A.}}$ diagonal for both collision energies. This diagonal line describes 77.4% of the 35 MeV/nucleon data and 76.2% of the 45 MeV/nucleon

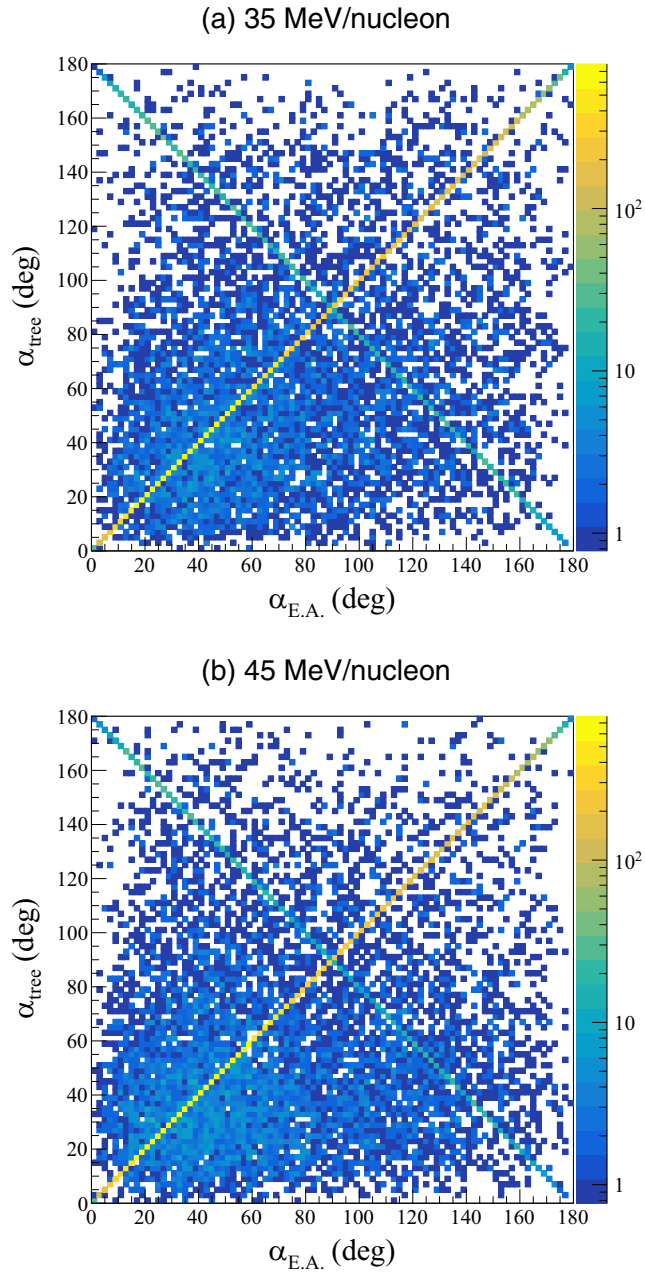

FIG. 5. Angular alignments calculated by each of the two methods for the (a) 35 and (b) 45 MeV/nucleon data. A primary peak is shown along the main diagonal, $\alpha_{\text{tree}} = \alpha_{\text{E.A.}}$. A secondary peak is populated on the off diagonal $\alpha_{\text{tree}} = 180° - \alpha_{\text{E.A.}}$. There are also large amount of the data on neither diagonal.

data. A secondary peak is also observed along the line $\alpha_{\text{tree}} = 180° - \alpha_{\text{E.A.}}$. This peak is much less prominent than the primary peak, describing only 0.63% of the 35 MeV/nucleon data and 0.48% of the 45 MeV/nucleon data. There are also a large number of events where the two methods display no obvious correlation. The origins of these features give important insight to key differences between the experimental assumptions and the even-tree method.

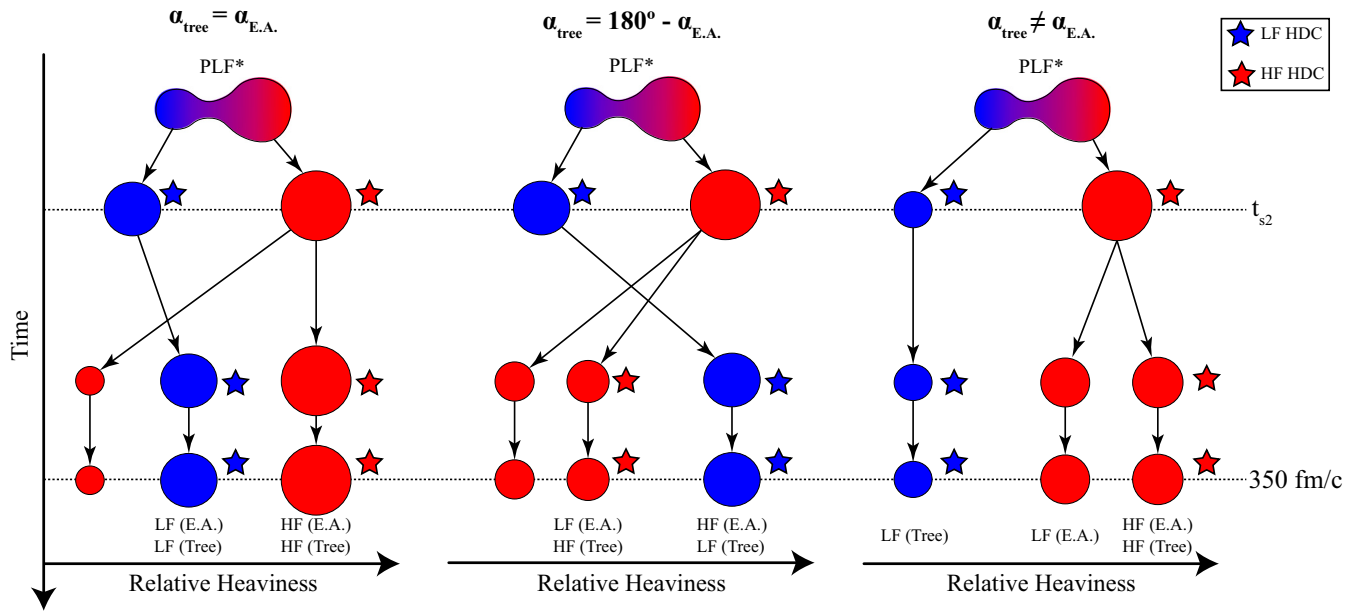

FIG. 6. Depictions of how a PLF* decaying multiple times may cause different types of disagreement between the event tree analysis and experimental assumptions.

These types of discrepancies are the result of a PLF* which emits multiple light fragments during its de-excitation. In Fig. 6, multiple cases are illustrated, which each corresponding to a region of the α_{tree} versus $\alpha_{\text{E.A.}}$ distributions. In each of these diagrams, the PLF* breaks apart into an HF and LF, but then the HF breaks apart further into two fragments. In the leftmost case, the HF simply emits a fragment lighter than the original LF; the resulting α_{tree} and $\alpha_{\text{E.A.}}$ are calculated from the same fragments. Events with an HF that decays in this way or not at all will populate the main diagonal in Fig. 5. If, however, the HF breaks apart such that all of its daughters are lighter than the LF (middle panel of Fig. 6), then the identities of the HF and LF found by the tree will be the same as the fragments identified by the experimental methods, but they will be switched. Events like this populate the supplementary angle peak in Fig. 5. Note that the fragment that was the light partner at the time of the PLF* breakup is correctly identified as the LF when the tree method is implemented. Finally, it is possible that the original LF is lighter than both of the HF's daughters. In this case, the two methods would agree on the HF identification, but pick two entirely different LFs with different trajectories. This simply results in the events on neither diagonal, as the two α values are corresponding to separate breakup events, with effectively different t_{s2} values. The Δt calculated for an event will still correspond to the initial PLF* breakup, and the relationship between α and PLF* lifetime are preserved by the tree method.

IV. MODELING THE ANGULAR ALIGNMENT DISTRIBUTIONS

The alignment distributions have contributions from isotropic, statistical decay following an approximately $\sin\alpha$ distribution and a dynamic peak associated with the events where neutron-proton equilibration is most prominent. The functional form chosen to model the dynamic yield is shown in Eq. (8):

$$Y_{\text{dyn}}(\alpha) = \frac{\alpha}{\lambda^2}\exp\left(-\frac{\alpha^2}{2\lambda^2}\right). \tag{8}$$

The fit parameter, λ, describes both the width and the mean value in the dynamic peak. The yield of the total α distribution is modeled by

$$Y(\alpha) = \frac{A}{2}\sin\alpha + BY_{\text{dyn}}(\alpha) + CY_{\text{dyn}}(180^\circ - \alpha), \tag{9}$$

which was used to fit the data shown in Fig. 4 with four parameters. The coefficients A, B, and C, are related to the relative yield of the statistical, dynamic, and peak associated with the dynamic events with an inverted $\vec{v}_{\text{rel}}$. The contribution to the flipped term in the experimental assumptions is in part due to ternary decay.

It is also possible that the component of the PLF* associated with the LF breaks off as the heavier component, especially in nearly symmetric PLF* breakups with $Z_{\text{LF}} \approx Z_{\text{HF}}$. Figure 7 shows how the ratio C/B depends on the parameter

$$\eta \equiv \frac{Z_{\text{HF}} - Z_{\text{LF}}}{Z_{\text{HF}} + Z_{\text{LF}}}, \tag{10}$$

which is a measure of the charge asymmetry of the PLF* breakup. In all four data sets, when the breakup is very symmetric ($\eta \approx 0$), the ratio of C/B approaches nearly 1. The daughter associated with the originally more neutron-rich region of the PLF* is taken as the lighter of the two heaviest daughters of the PLF*. This means that if the LF and the HF happen to be similar in size, they can be confused, resulting

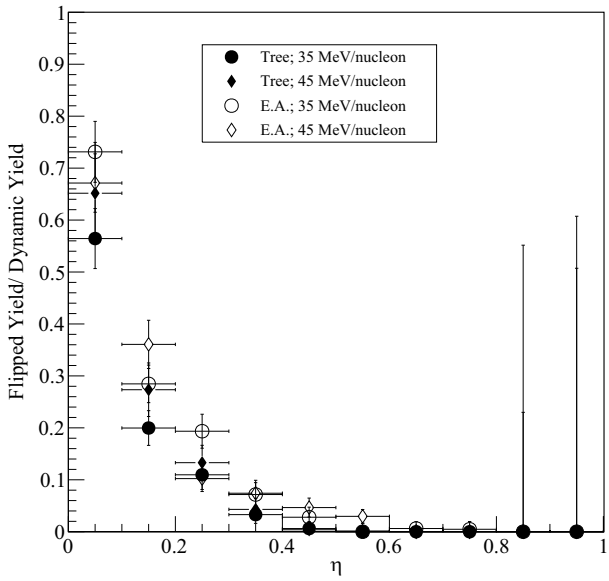

FIG. 7. Ratio of yields from the flipped peak to the dynamic peak as a function of the charge asymmetry of the PLF* breakup.

in an enhancement of C/B at low η. This general trend can is supported by data presented in Refs. [15,26]. Conversely, one notices that as η increases to 1 (asymmetric breakup), the yield in the dynamic term dominates over the flipped term and C/B goes to 0 for all data sets. We note that $B > C$ for the entire domain of η, and the dynamic peak dominates the flipped peak by a factor of 10 or more for $\eta \geqslant 0.4$.

V. CHARACTERIZING DYNAMIC BREAKUP WITH RESPECT TO TIME

In prior work [14,25], the angular frequency, ω, of the PLF* formed in collisions of $^{70}\mathrm{Zn} + {}^{70}\mathrm{Zn}$ at 35 MeV/nucleon was found using a classical approximation, $\omega = L/I$, where L is the angular momentum of the fragment, and I is its moment of inertia. The moment of inertia was estimated by assuming that the PLF* was comprised of two rigid touching spheres with radii corresponding to the HF and LF nucleon number, leading to values of inertia in the range of 2.8–9.9(10^{-42} MeVs^2). An estimate of $L = 22\hbar$ was used resulting in an estimated angular frequency of 1.5 rad/zs $\leqslant \omega \leqslant$ 5.2 rad/zs.

We use the event-tree analysis to relate Δt and α_{tree} for each event. As neutron-proton equilibration is seen particularly in PLF*s which break apart dynamically, the expected α value in the dynamic peak is predicted to have a relationship with time. The angular distribution from the tree analysis may be partitioned into intervals of Δt separated by 10 fm/c (governed by the interval between output time steps). In each of these time windows, the α_{tree} distribution was fit with the functional form of Eq. (9). This fit can then be used to derive the average angular alignment in the dynamic component of the distribution by integration of Eq. (9) as given by Eq. (11):

$$\langle\alpha\rangle_{\mathrm{dyn}} = \frac{\int_0^\infty \alpha Y_{\mathrm{dyn}}(\alpha)d\alpha}{\int_0^\infty Y_{\mathrm{dyn}}(\alpha)d\alpha} = \sqrt{\frac{\pi}{2}}\lambda. \qquad (11)$$

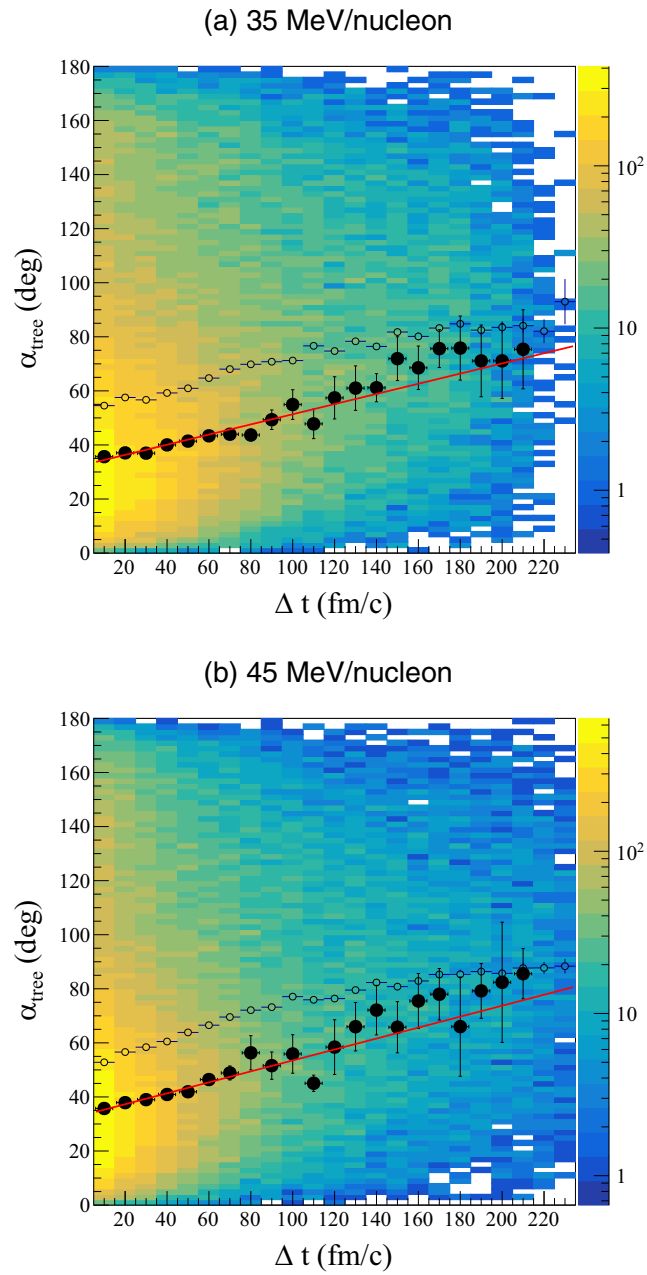

FIG. 8. The angular alignment is plotted against the time between the PLF*/TLF* breakup and HF/LF breakup for the 35 and 45 MeV/nucleon collision energies. The determinations of $\langle\alpha_{\mathrm{dyn}}\rangle$ for each Δt are plotted as solid black points. The data are fitted linearly and the average values of the total yield, $\langle\alpha\rangle$, are also plotted as open circles.

Figure 8 shows the alignment angle α_{tree} versus Δt for both collision energies. This plot is in qualitative agreement with results in [26], which used antisymmetrized molecular dynamics simulations. The average alignment angles, $\langle\alpha\rangle$, are plotted as open points in each bin of Δt. Additionally, the average alignment in the dynamic peak, $\langle\alpha\rangle_{\mathrm{dyn}}$, are plotted in solid data points. Only points which have a dynamic peak inconsistent with 0 are used (require $B > \sigma_B$ from the fit). We

TABLE I. Effective rotational speeds of the excited PLF* for different energies of ^{70}Zn + ^{70}Zn collisions.

Energy (MeV/nucleon)	ω_{eff} (rad zs^{-1})	$\langle\alpha\rangle_{\text{dyn},0}$ (deg)
35	0.98 ± 0.08	32.5 ± 0.7
45	1.06 ± 0.09	33.3 ± 0.7

note that by about 220 fm/c this condition fails as the dynamic yield is relatively small and our sample size is limited at this extreme. The correlation of $\langle\alpha\rangle$ and Δt is approximately linear between 0 and 100 fm/c, where it begins to plateau to 90° as the statistical contribution dominates. Notice, that there is an apparent correlation between $\langle\alpha\rangle_{\text{dyn}}$ and Δt which is approximately linear for both collision energies. Both $\langle\alpha\rangle$ and $\langle\alpha\rangle_{\text{dyn}}$ have approximately the same slope with small Δt where dynamic decay dominates, but have different offsets due to the removal of the statistical component.

A quantitative relationship between the dynamic term and the PLF* lifetime is extracted through a linear fit, Eq. (12), to the $\langle\alpha\rangle_{\text{dyn}}$ versus Δt data:

$$\langle\alpha\rangle_{\text{dyn}} = \langle\alpha\rangle_{\text{dyn},0} + \omega_{\text{eff}}\Delta t. \tag{12}$$

The fit results are shown in Table I. The parameter ω_{eff} represents a metric to test the existence of the angular alignment's dependence on dynamically decaying PLF*'s lifetime. For both collision energies, the parameter ω_{eff} was found at both energies to be about 1.0 rad/zs, which is different than 0 with convincing statistical significance (over 10σ). This affirms that there is a correlation between $\langle\alpha\rangle_{\text{dyn}}$ and Δt.

The magnitude of this dependence did not vary in any appreciable way between the two energies, and was reasonably close the lower limit of values utilized by previous experimental work [14,25]. Additionally, the dependence demonstrated here is even more supportive of the proposed description of the dynamic decay process than just the effects of the relative dynamic yield decreasing with PLF* lifetime.

VI. SUMMARY

A new event tree method of analyzing molecular dynamics simulations to study collision dynamics has been presented. The CoMD model used here provides accurate distributions of fragment masses and velocities. Moreover, it handles the collision dynamics well allowing at all times dynamical breakup and therefore also providing good relative velocity distribution and good angular distributions. Because of the way CoMD explicitly enforces Pauli blocking, it is fast to run which allows for obtaining a large sample size necessary for the present analysis. This analysis method investigates the correlation between the lifetime of excited projectilelike fragments and the angular alignment of their largest daughters. The analysis method uses the positions of nucleons at discrete times during the reaction. At each time step, nuclear clusters are identified, and the parents and daughters of the each cluster are found by comparing the nucleon content of each cluster in adjacent time steps. Through this, the lifetime of the PLF* from its formation to its binary breakup is calculated.

The alignment angle distribution is deconvoluted into its statistical and dynamical components, and the mean alignment angle of the dynamical component is compared to the PLF* lifetime. A linearly increasing correlation is observed with a slope of approximately 1 rad/zs. This is true for both collision energies in this study (35 and 45 MeV/nucleon). The rotational speed calculated here helps validate the values implemented in analysis of experimental results in Refs. [14,25]. The demonstration of this effective rotational speed connecting PLF* lifetime and angular alignment is encouraging: this lends support that the mechanism proposed to explain the experimental results is borne out in the dynamical simulation. Further, this opens the door to future studies of the dynamical decay mechanism, such as the concurrent neutron-proton equilibration. The observables focused on in this study may be sensitive to the symmetry energy. In principle, by comparison of experimental data to dynamical simulations in which the equation of state is varied, it may be possible to probe the asymmetry energy at subsaturation density. Such results are model dependent, and the observables can be impacted by more than one ingredient in the model. Therefore, not only are new high resolution experiments necessary, but reliably constraining the EOS may require significant effort in theoretical developments to allow multiple models to simultaneously describe multiple observables across multiple beams, targets, and energies.

ACKNOWLEDGMENTS

This work was made possible by support from the NSF (Grant No. PHY-1659847), Robert A. Welch Foundation (Grant No. A-1266), and DOE (Grants No. DE-FG02-93ER40773 and No. DE-NA0003841).

[1] P. Danielewicz, R. Lacey, and W. G. Lynch, Determination of the equation of state of dense matter, Science **298**, 1592 (2002).

[2] B.-A. Li, L.-W. Chen, and C. M. Ko, Recent progress and new challenges in isospin physics with heavy-ion reactions, Phys. Rep. **464**, 113 (2008).

[3] C. Fuchs and H. H. Wolter, Modelization of the EoS, Eur. Phys. J. A **30**, 5 (2006).

[4] D. V. Shetty, S. J. Yennello, and G. A. Souliotis, Density dependence of the symmetry energy and the nuclear equation of state: A dynamical and statistical model perspective, Phys. Rev. C **76**, 024606 (2007).

[5] A. B. McIntosh and S. J. Yennello, Interplay of neutron-proton equilibration and nuclear dynamics, Prog. Part. Nucl. Phys. **108**, 103707 (2019).

[6] P. Napolitani and M. Colonna, Frustrated fragmentation and reaggregation in nuclei: A nonequilibrium description in spallation, Phys. Rev. C **92**, 034607 (2015).

[7] A. Bromley (ed.), *Treatise on Heavy-Ion Science*, Vol. 2: Fusion and Quasifusion Phenomena (Springer, Berlin, 1985).

[8] L. Shvedov, M. Colonna, and M. Di Toro, Breakup mechanisms in heavy-ion collisions at low energies, Phys. Rev. C **81**, 054605 (2010).

[9] P. Napolitani and M. Colonna, Dynamical description of heavy-ion collisions at fermi energies, EPJ Web Conf. **117**, 07008 (2016).

[10] J. Colin *et al.* (INDRA Collaboration), Dynamical effects in multifragmentation at intermediate energies, Phys. Rev. C **67**, 064603 (2003).

[11] V. Baran, M. Colonna, V. Greco, and M. Di Toro, Reaction dynamics with exotic nuclei, Phys. Rep. **410**, 335 (2005).

[12] D. Thériault *et al.*, Neutron-to-proton ratios of quasiprojectile and midrapidity emission in the ^{64}Zn $+^{64}$Zn reaction at 45 MeV/nucleon, Phys. Rev. C **74**, 051602(R) (2006).

[13] S. Hudan *et al.*, Tracking saddle-to-scission dynamics using n/z in projectile breakup reactions, Phys. Rev. C **86**, 021603(R) (2012).

[14] A. Rodriguez Manso, M. A. B., A. Jedele, K. Hagel, L. Heilborn, Z. Kohley, L. W. May, A. Zarrella, and S. J. Yennello, Detailed characterization of neutron-proton equilibration in dynamically deformed nuclear systems, Phys. Rev. C **95**, 044604 (2017).

[15] A. B. McIntosh *et al.*, Short-lived binary splits of an excited projectile-like fragment induced by transient deformation, Phys. Rev. C **81**, 034603 (2010).

[16] A. B. McIntosh, Binary and ternary breakup of excited projectile-like fragments produced intermediate collisions of ^{124,136}Xe nuceli with ^{112,124}Sn targets at $E/A = 50$ MeV, Ph.D. thesis, Indiana University, 2010.

[17] P. Russotto *et al.*, Dynamical versus statistical production of intermediate mass fragments at fermi energies, Eur. Phys. J. A **56**, 12 (2020).

[18] E. De Filippo *et al.*, Correlations between emission timescale of fragments and isospin dynamics in ^{124}Sn$+^{64}$Ni and ^{112}Sn$+^{58}$Ni reactions at 35*a* MeV, Phys. Rev. C **86**, 014610 (2012).

[19] C. P. Montoya *et al.*, Fragmentation of Necklike Structures, Phys. Rev. Lett. **73**, 3070 (1994).

[20] B. Davin *et al.*, Fragment production in noncentral collisions of intermediate-energy heavy ions, Phys. Rev. C **65**, 064614 (2002).

[21] E. De Filippo *et al.*, Time sequence and timescale of intermediate mass fragment emission, Phys. Rev. C **71**, 044602 (2005).

[22] K. Brown, S. Hudan, R. T. deSouza, J. Gauthier, R. Roy, D. V. Shetty, G. A. Souliotis, and S. J. Yennello, Timescale for equilibration of n/z gradients in dinuclear systems, Phys. Rev. C **87**, 061601(R) (2013).

[23] K. Stiefel, Z. Kohley, R. T. deSouza, S. Hudan, and K. Hammerton, Symmetry energy dependence of long-timescale isospin transport, Phys. Rev. C **90**, 061605 (2014).

[24] S. Hudan and R. T. deSouza, Timescale for isospin equilibration in projectile breakup, Eur. Phys. J. A **50**, 36 (2014).

[25] A. Jedele, A. B. McIntosh, K. Hagel, M. Huang, L. Heilborn, Z. Kohley, L. W. May, E. McCleskey, M. Youngs, A. Zarrella, and S. J. Yennello, Characterizing Neutron-Proton Equilibration in Nuclear Reactions with Subzeptosecond Resolution, Phys. Rev. Lett. **118**, 062501 (2017).

[26] S. Piantelli *et al.*, Dynamical fission of the quasiprojectile and isospin equilibration for the system ^{80}Kr $+^{48}$Ca at 35 MeV/nucleon, Phys. Rev. C **101**, 034613 (2020).

[27] A. Hannaman *et al.*, Isoscaling and nuclear reaction dynamics, Phys. Rev. C **101**, 034605 (2020).

[28] L. Beaulieu *et al.*, Signals for a Transition from Surface to Bulk Emission in Thermal Multifragmentation, Phys. Rev. Lett. **84**, 5971 (2000).

[29] G. A. Souliotis, D. V. Shetty, M. Veselsky, G. Chubarian, L. Trache, A. Keksis, E. Martin, and S. J. Yennello, Isotopic scaling of heavy projectile residues from the collisions of 25 MeV/nucleon ^{86}Kr with ^{124}Sn, ^{112}Sn and ^{64}Ni, ^{58}Ni, Phys. Rev. C **68**, 024605 (2003).

[30] M. B. Tsang *et al.*, Isospin Diffusion and the Nuclear Symmetry Energy in Heavy Ion Reactions, Phys. Rev. Lett. **92**, 062701 (2004).

[31] J. Galin, B. Gatty, D. Guerreau, M. Lefort, X. Tarrago, R. Babinet, B. Cauvin, J. Girard, and H. Nifenecker, The transition between quasi elastic and completely damped collisions studied in the ^{40}Ar (280 MeV)+^{58}Ni reaction, Z. Phys. A: At. Nucl. **278**, 347 (1976).

[32] J. V. Kratz, H. Ahrens, W. Bögl, W. Brüchle, G. Franz, M. Schädel, I. Warnecke, G. Wirth, G. Klein, and M. Weis, Charge-Asymmetry Equilibration in the Reaction of ^{129,132,136}Xe with ^{197}Au Near the Interaction Barrier, Phys. Rev. Lett. **39**, 984 (1977).

[33] G. J. Mathews, J. B. Moulton, G. J. Wozniak, B. Cauvin, R. P. Schmitt, J. S. Sventek, and L. G. Moretto, ^{20}Ne-induced reactions with Cu and ^{197}Au at 8.6 and 12.6 MeV/nucleon, Phys. Rev. C **25**, 300 (1982).

[34] H. Freiesleben and J. Kratz, Nz-equilibration and nucleon exchange in dissipative heavy-ion collisions, Phys. Rep. **106**, 1 (1984).

[35] E. Hernandez, W. Myers, J. Randrup, and B. Remaud, Quantal dynamics of charge equilibration in damped nuclear collisions, Nucl. Phys. A **361**, 483 (1981).

[36] L. G. Moretto and R. P. Schmitt, Deep inelastic reactions: A probe of the collective properties of nuclear matter, Rep. Prog. Phys. **44**, 533 (1981).

[37] D. Gruyer *et al.* (INDRA Collaboration), Coulomb chronometry to probe the decay mechanism of hot nuclei, Phys. Rev. C **92**, 064606 (2015).

[38] H.-S. Wang, J. Xu, B.-A. Li, and W.-Q. Shen, Reexamining the isospin-relaxation time in intermediate-energy heavy-ion collisions, Phys. Rev. C **98**, 054608 (2018).

[39] M. Papa, T. Maruyama, and A. Bonasera, Constrained molecular dynamics approach to fermionic systems, Phys. Rev. C **64**, 024612 (2001).

[40] M. Papa, G. Giuliani, and A. Bonasera, Constrained molecular dynamics II: An n-body approach to nuclear systems, J. Comput. Phys. **208**, 403 (2005).